Silicon (2018) 10:1679–1686
https://doi.org/10.1007/s12633-017-9652-8

ORIGINAL PAPER

Role of Temperature on the Phase Modification of TiO_2 Nanoparticles Synthesized by the Precipitation Method

T. Kalaivani[1,2] · P. Anilkumar[3]

Received: 16 May 2017 / Accepted: 2 October 2017 / Published online: 29 December 2017

Abstract Nanostructured TiO_2 samples have been synthesized successfully by a simple precipitation method. The prepared samples are characterized by X-ray diffraction (XRD), transmission electron microscopy (TEM), Fourier transform infrared (FTIR), photoluminescence (PL) spectroscopy, ultra violet (UV) spectroscopy and Raman spectroscopy respectively. The as-prepared TiO_2 nanoparticls appear to be a single anatase phase with average crystalline size 37.68 nm at 150 °C and found to be transformed from anatase to rutile phase during the annealing of samples in the temperature range from 150 °C to 600 °C. The TEM images indicate the particle sizes are in the range between 12 and 25 nm for anatase phase TiO_2 at 400 °C and 30–45 nm for rutile phase TiO_2 at 600 °C. The luminescence property of the TiO2 nanoparticles studied by the emission properties confirms the presence of defect levels caused by the oxygen vacancies. Raman spectroscopy was used to identify and quantity the amorphous and crystalline TiO_2 phases. FTIR studies reveal weak complex vibrations between the titanium and oxygen species and also additional unsaturated sites (Ti^{3+}) through incorporation of (OH) groups, not otherwise seen in bulk TiO_2.

✉ P. Anilkumar
anilk612@gmail.com; kalaibu17@gmail.com

[1] Department of Chemistry, Research and Development Centre, Bharathiar University, Coimbatore 641046, Tamilnadu, India

[2] Department of Chemistry, VSB Engineering College, Karur-639 111, Tamilnadu, India

[3] Department of Chemistry, KPR Institute of Engineering and Technology, Coimbatore 641 407, Tamilnadu, India

Keywords TiO_2 nanoparticles · XRD · TEM · UV · PL · FTIR · Raman spectroscopy

1 Introduction

Particles smaller than tens of nanometers in primary particle diameter are of interest for the synthesis of new materials because of their low melting point, special optical properties, high catalytic activity and unusual mechanical properties compared with their bulk material counterpart [1]. In recent years applications of nanoparticles are getting more generalized covering different fields including optoelectronics [2], catalysis [3], medicine [4] and sensor devices [5, 6] among the bulk materials. Parameters like structure, size and elemental composition are considered to be important besides the quantum size effects in materials of nanometer scale for their promising applications. Controlling size plays a major role in catalysis application and controlling their shape plays a vital role in fabrication of photonic crystals [7].

In recent years titanium dioxide (TiO_2) is used as one of the most interesting nanostructured materials because of its excellent optical, electrical and catalytic properties [8]. In general TiO_2 exhibits three crystalline phases, anatase, rutile and brookite [9]; among the phases, anatase and rutile are relevant for a variety of technological applications [10] between which anatase TiO_2 is of stronger current interest especially in the surface chemistry field due to its higher catalytic activity [11]. With increase in calcination temperature the anatase phase transforms to the rutile phase [12, 13]. The applications such as dye sensitized solar cell (DSSC), photocatalysis and gas sensors are found to depend strongly on the crystalline structure, morphology and particle size of titania nanoparticles [14]. Several synthesis methods have been proposed to prepare TiO_2 nanoparticles,

such as sol-gel [15], thermal hydrolysis [16], hydrothermal processing [17], chemical vapour deposition [18], and thermal plasma approach [19]. Specially the sol–gel method offers to synthesize high active anatase phase TiO_2 with important advantages over other techniques due to excellent compositional control, high homogeneity at the molecular level, lower crystallization temperature and feasibility of producing ultrafine nanoparticles [20]. Among the synthetic approaches the coprecipitation method is considered to be one of the best techniques and potentially advantageous in comparison to other methods to produce pure phase formation of compounds, low temperature preparation, high purity and yield of nanoparticles.

The present work is an attempt to prepare anatase to rutile phases of TiO_2 nanopaticles. The prepared samples are characterized for their thermal analysis, structural, morphology and optical properties.

2 Experimental Details

All the chemicals used for synthesizing TiO_2 nanoparticles were of analytical reagent grade (99% purity procured from Sigma Aldrich). Nanostructured TiO_2 samples were prepared using the precursor titanium isopropoxide and isopropyl alcohol. 50 ml of isopropyl alcohol was added to 10 ml of titanium isopropoxide and stirred for 30 min. 0.1 g of PVP solution was also prepared. The prepared polyvinylpyrrolidone (PVP) solution was added to the above solution and then stirred for 20 min. For the hydrolysis reaction 100 ml of deionized water was added dropwise to the mixed solution. The resulting white precipitate of $Ti(OH)_4$ is refluxed for 2 h and then stirred continuously for 12 h. Finally, the precipitate is centrifuged with deionized water and ethanol to remove impurities. After centrifuging, the white precipitate is dried at 150 °C for 3 h and the fine powder was washed with double distilled water. Finally, the as-prepared $Ti(OH)_4$ precipitate was annealed at various temperatures from 300 to 600 °C in steps of 100 °C to obtain TiO_2 nanoparticles.

The as-prepared and annealed samples are characterized for their purity and crystallinity by X-ray powder diffraction (XRD) using a XPERT-PRO, Bruker AXS D8 Advance X-ray diffractometer. Transmission electron microscopy (TEM) used a JEOL Model JSM—6390LV instrument for high resolution surface imaging and a Philips CM20 super twin microscope, respectively. Specimens for TEM are prepared by ultrasonic dispersion of the powder sample in ethanol and putting a droplet of the suspension on a copper microscope grid covered with carbon. IR spectra are taken with a Bruker IFSTable 88 spectrometer in the range 4000–400 cm^{-1}. The room temperature photoluminescence spectra were obtained on a spectrofluorimeter (Fluorolog Model FL3-11). The optical studies of the samples were done with a UV-Vis spectrophotometer (Model JASCO-V-570) in the range from 300 to 900 nm. FT-Raman spectra were obtained at room temperature using a Bruker FRA 106/S FT-Raman spectrometer equipped with an InGaAs detector. The radiation from a Nd-YAG laser (1.5 W) was used as the excitation source. TG/DTA measurements are carried out with the help of SII nanotechnology, TG/DTA 6200 in nitrogen atmosphere. Samples weighing 20.0 ± 0.1 mg are heated in a ceramic sample boat up to 900 °C at 20 °C/min in a stream (40 ml/min) of nitrogen gas.

3 Results and Discussion

3.1 Structural Properties of TiO_2 Nanoparticles

The X-ray diffraction patterns of as-prepared TiO_2 nanoparticles at 150 °C with various temperatures from 300 to 600 °C are shown in Fig. 1. It is observed that (Fig. 1a–c) the anatase and rutile TiO_2 nanoparticles are polycrystalline in nature with tetragonal crystal structure having preferential orientation growth along the (101) plane and other peaks are associated with the (101), (110), (103), (004), (112), (200), (105), (211), (204), (116), (220), (215) and (301) planes for anatase TiO_2 and (110), (101), (200), (111), (211), (211), (220), (002), (310), (301), (112) and (202) planes for rutile

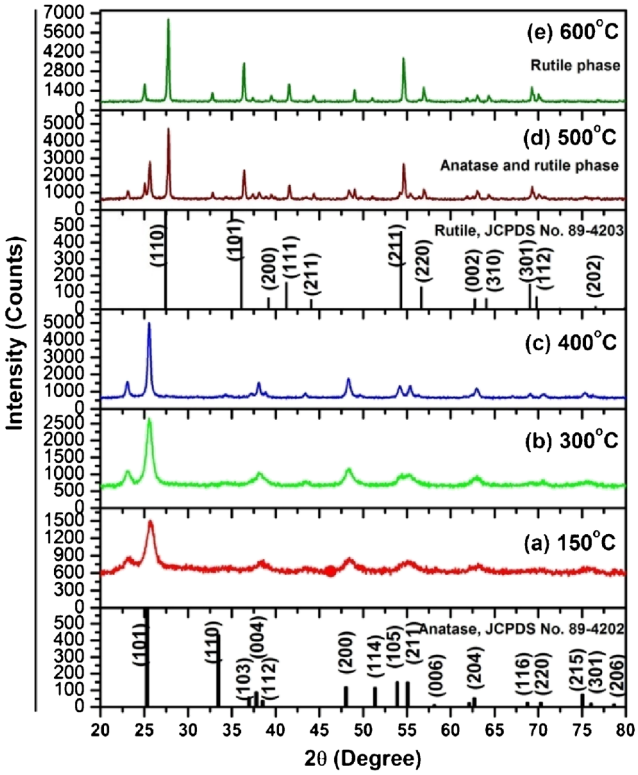

Fig. 1 XRD pattern of TiO_2 nanopaticles

TiO_2 nanoparticles. The observed diffraction peak patterns were compared with standard diffraction values of JCPDS (Card Nos. 89-4202 and 89-4203). It is seen from Fig. 1, the anatase to rutile TiO_2 can be detected, which can be attributed to the contribution of the low concentration of oxygen vacancies due to the high concentration of gaseous oxygen during particle growth hindering the transformation from anatase to rutile phase. It is very important to note that annealing temperature increases with the phase shift from anatase to rutile. The lattice parameters of TiO_2 nanoparticles were evaluated using Eq. 1.

$$\frac{1}{d^2} = \frac{(h^2 + k^2)}{a^2} + \frac{l^2}{c^2} \tag{1}$$

where, d is the interplanar spacing and (h,k,l) are Miller indices. It can be seen from Table 1 that all the samples have good agreement with the TiO_2 lattice parameters ($a = 3.2497$ Å and $c = 5.2018$ Å) with tetragonal structure. The crystallite size of TiO_2 nanoparticles was evaluated using Eq. 2.

$$D = \frac{0.94\lambda}{\beta \cos\theta} \tag{2}$$

where, D is the grain size of crystallite, λ is the wavelength of X-rays, β is the broadening of the diffraction line measured at half its maximum intensity in radians and θ is the angle of diffraction. The variation of crystallite size with temperature of TiO_2 nanoparticles is listed in Table 1. From Table 1, it is observed that the crystallite size increases with temperature increase up to 400 °C and attains a maximum 19 nm at 400 °C and 39 nm at 600 °C for rutile phase TiO_2 nanoparticles. A sharp increase in crystallite size and

Table 1 The structural analysis of TiO_2 nanoparticles

Temperature (°C)	Pos. [2θ]	d-spacing [Å]	FWHM [2θ]	hkl	Lattice constant (Å)		Crystalline size (nm)	Microstrain (ε) 10^4 $lin^{-2}m^{-4}$	Dislocation density (δ)
					a	c			10^{14} lin/m^2
150 °C	25.698	3.4666	0.6326	101	3.7738	9.3923	13.444	26.9	5.52
	38.386	2.3450	1.0775	112			10.330	3.19	0.07
	48.469	1.8781	0.3238	200			28.094	1.28	1.26
	55.071	1.6676	0.2078	211			45.018	0.80	0.49
	63.275	1.4697	0.6972	204			13.974	2.59	5.12
300 °C	25.580	3.4824	0.8571	101	3.7745	9.4471	9.9244	3.64	10.1
	38.127	2.3603	1.0460	112			8.3905	4.31	14.2
	48.367	1.8818	1.2450	200			7.2993	4.95	18.7
	55.280	1.6618	1.0649	211			8.7931	4.11	12.9
	62.984	1.4758	0.4239	204			22.948	1.55	1.89
400 °C	25.557	3.4855	0.4270	101	3.7687	9.5024	19.920	1.81	2.52
	38.074	2.3635	0.3557	112			24.670	1.46	1.64
	48.320	1.8836	1.0200	200			15.580	0.79	0.04
	55.350	1.6598	0.4745	211			19.740	1.83	2.56
	62.963	1.4762	0.5458	204			17.821	2.03	3.18
500 °C	27.760	3.2136	0.2023	110	4.5812	2.9260	42.237	8.56	0.56
	36.413	2.4674	0.2360	101			37.001	9.78	0.73
	41.591	2.1714	0.8460	111			10.488	3.45	9.09
	54.648	1.6795	0.2730	211			55.709	2.82	0.06
	69.322	1.3555	0.2879	301			35.029	12.3	0.81
600 °C	27.731	3.2169	0.2029	110	4.5801	2.9300	42.110	8.59	0.56
	36.381	2.4695	0.2166	101			40.312	8.97	0.61
	41.549	2.1735	0.2225	111			39.874	9.07	0.62
	54.639	1.6797	0.2106	211			44.333	8.16	0.50
	69.317	1.3556	0.3392	301			29.730	12.1	1.13

decrease in dislocation density and microstrain with temperature is noted. The dislocation density and microstrain were calculated using the following Eqs. 3 and 4;

$$\delta = \frac{1}{D^2} \tag{3}$$

$$\varepsilon = \frac{\beta \cos \theta}{4} \tag{4}$$

For the sample at temperature 600 °C, the minimum values for dislocation density and microstrain probability of the sample (Table 1) are obtained. The TiO_2 nanoparticles with lower microstrain and dislocation density improve the crystallinity of the nanoparticles. The lattice constants (a, c), crystallite size, microstrain, and dislocation density results of the nanoparticles are given in Table 1. It is concluded from the structural analysis that the increase of film thickness has a strong effect on the structural properties of the nanoparticles.

3.2 Transmission Electron Microscopy

Figure 2 shows different magnifications of TiO_2 nanoparticles at two temperatures, 400 °C and 600 °C. The transmission electron microscope analysis was carried out to confirm the particle sizes, growth orientation and distribution of the crystallites. It is evident from the micrographs that the average particle size increases with temperature. It is observed that (Fig. 2a) the surface of TiO_2 nanoparticles is uniform spherical grains. For the estimation of the average particle size of samples, a line was drawn on the TEM image and its length was divided by the number of grain boundaries crossing the line. The sample at 400 °C (Fig. 2a) shows the apparent polycrystalline surface with spherical-like structures having average particle size ∼10 nm. This size is slightly less than the particle size of 13 nm reported in the earlier work [21]. Further increase of the annealing temperature up to 600 °C, leads to the formation of spherical size structures with an average size of the particles ∼22 nm (Fig. 2b). The selected area electron diffraction (SAED) pattern (Fig. 2a and b) shows the distinct and good diffraction rings corresponding to the anatase and rutile phases. The intensity of the diffraction rings indicates that the particle crystallites have good crystalline nature and a narrow size distribution. Each ring in the SAED pattern can be assigned to the prominent diffraction peaks of anatase and rutile TiO_2. The measurement of d-spacing of the rings are assigned in the order (101), (004), (200), (105), (211), (204), (116), (220) and (215) for anatase TiO_2 and (110), (101) (111), (211), (220) (002) (310) and (301) for rutile TiO_2 nanoparticles, respectively.

3.3 Optical Properties of TiO_2 Nanoparticles

3.3.1 FTIR Studies

The FTIR spectra of TiO_2 nanoparticles as prepared at 150 °C and annealed at various temperatures from 300

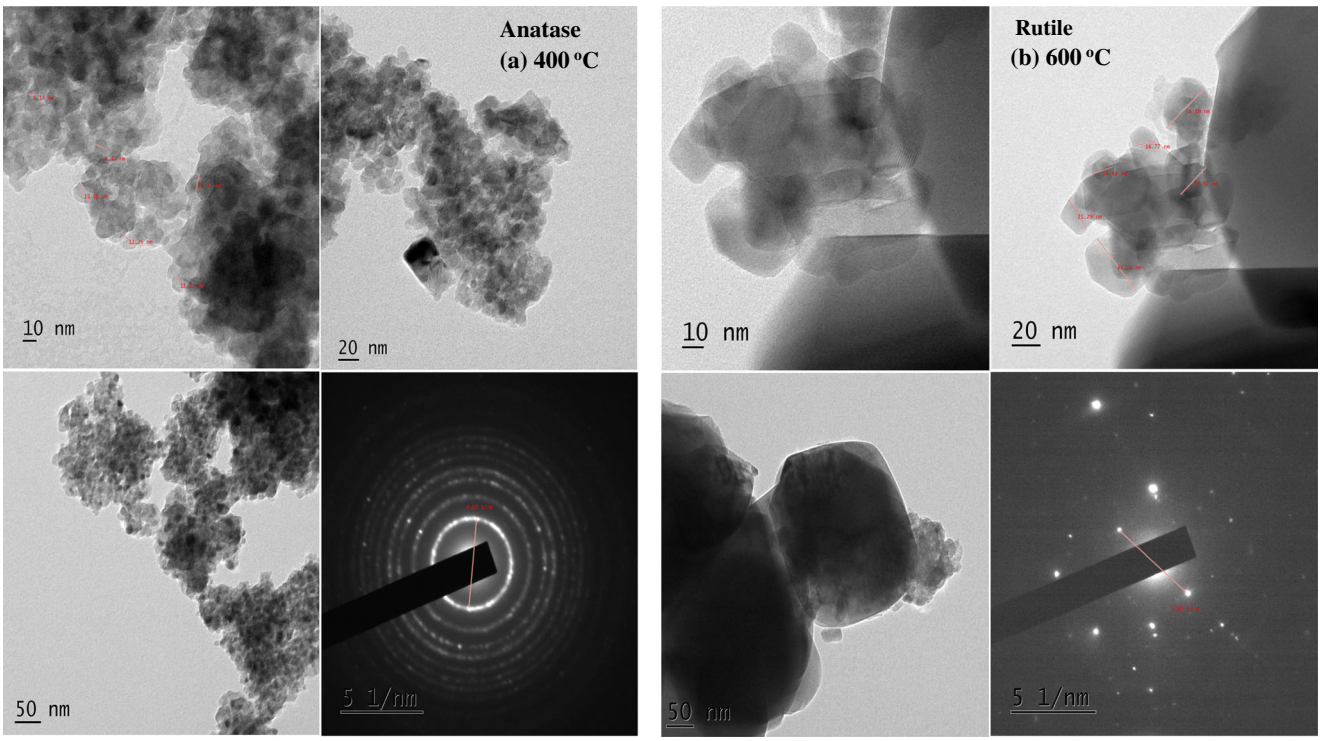

Fig. 2 TEM images of TiO_2 nanoparticles **a** anatase TiO_2 at 400 °C with SEAD pattern **b** Rutile TiO_2 at 600 °C with SEAD pattern

to 600 °C are shown in Fig. 3. Figure 3 corresponds to spectra recorded in the wavelength range 400–4000 cm^{-1} for the TiO_2 nanoparticles. In all the spectra the bands observed at 3400 and 1400 cm^{-1} were assigned to the presence of the −OH group of absorbed water and hydroxyl group on the surface. The spectrum band observed around 1600 cm^{-1} was due to the bending vibration of the -OH bond of chemisorbed water and the band observed around 3400 cm^{-1} was due to the stretching mode of the −OH bond of free water. The absorption band observed in the entire spectra at 1140 to 1225 cm^{-1} is attributed to the Ti-O-Ti vibration [22, 23]. The wide absorption band observed in the spectral region of 500–900 cm^{-1} is related to Ti-O bonds in the homogeneous powder of TiO_2. The band obtained at 1140 to 1225 cm^{-1} indicates the presence of the semicrystalline anatase phase for TiO_2 and the band observed at 1085 cm^{-1} in all the spectra corresponds to the characteristic rutile peak [24].

3.3.2 Photoluminescence Study

Photoluminescence spectra recorded at room temperature of the synthesized TiO_2 nanoparticles at 150 °C and various temperatures from 300 to 600 °C are shown in Fig. 4 where the excitation wavelength is 325 nm. The emission spectra possess one sharp UV emission at 421 nm and one weak broad band peaking at 483 nm. Such dominant UV band peaking at 421 nm has been attributed to the radiative annihilation of excitations. In this case, the band peaking at 483 nm can be ascribed to electron transition mediated by defects levels in the band gap, such as oxygen vacancies formed during sample preparation. The charge carrier recombination in small semiconductor particles is the non-radiative path because of strong coupling of wave functions of trapped electrons and trapped holes with lattice photons [25, 26]. The energy values of the trap levels as found in the spectra are 2.94 eV and 2.56 eV, which are attributed to the singly ionized oxygen vacancy in the TiO_2 and the emission results from the non radiative recombination of a photo-generated hole with an electron occupying the oxygen vacancy. The vacancy level at 2.94 eV in TiO_2 has been earlier confirmed using femtosecond photo-generated charge dynamics in TiO2 clusters [27]. It is found that the excellent optical properties of TiO_2 films can play an important role in fabricating highly efficient optoelectronic devices.

3.3.3 UV Studies of TiO_2 Nanoparticles

Figure 5 shows typical absorption spectra of TiO_2 particles at 150 °C and various temperatures from 300 to 600 °C. In all the particles the absorption was measured in the range between 250–700 nm. It is shown that TiO_2 is an oxide semiconductor and its anatase form has an optical absorbance range around 384 nm, and band gap 3.2 eV. In the current measurement the onset of the absorption peak of maximum absorbance occurred at 372 nm for TiO_2. Further, it decreased with increasing annealing temperature. The TiO_2 sample at 150 °C shows the absorbance of 372 nm.

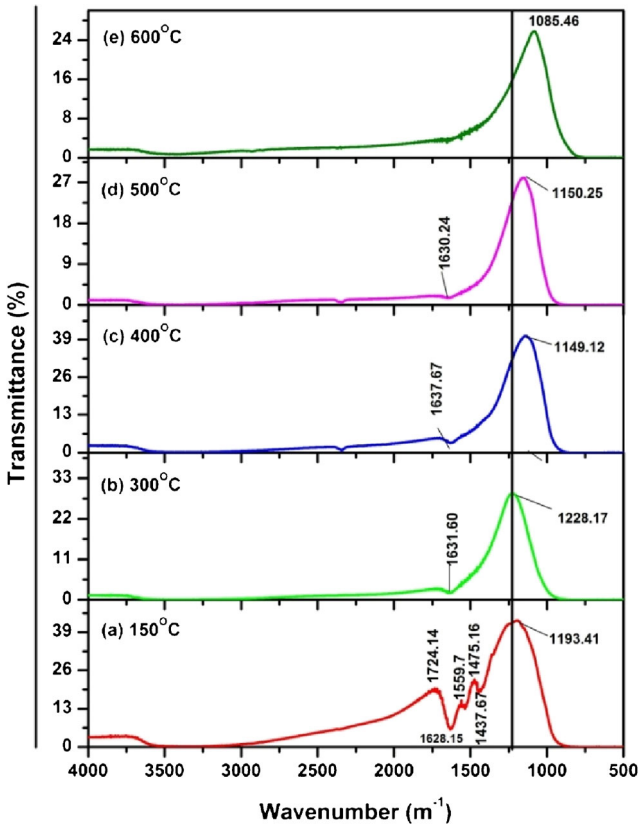

Fig. 3 FTIR spectra of TiO_2 nanoparticles

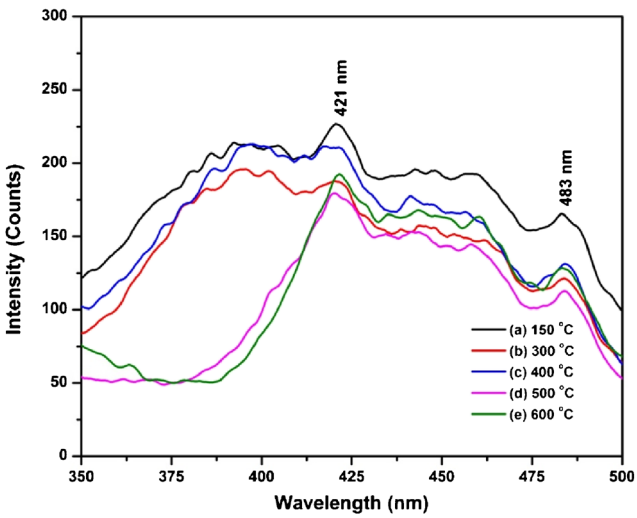

Fig. 4 PL spectra of TiO_2 nanoparticls

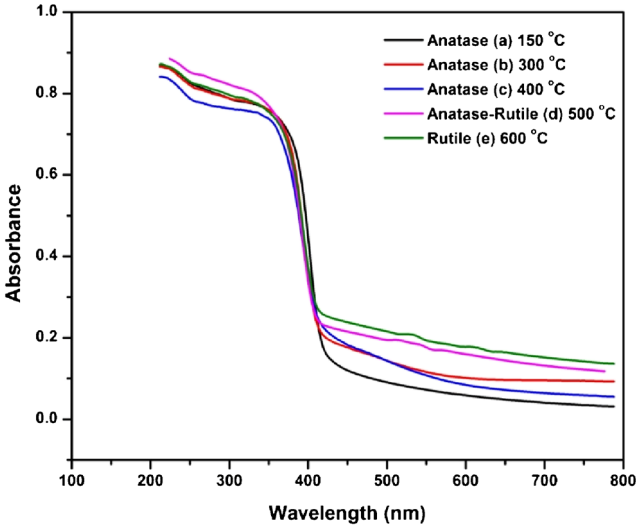

Fig. 5 UV absorbance spectra of TiO_2 nanoparticles

The absorbance was observed at 369, 360 and 350 nm for 300 °C, 400 °C and 500 °C respectively. The blue shift in absorbance corresponds to smaller particle size. The blue shift observed in the absorbance spectra indicated the quantum confinement effect [28]. The absorption edge shifting to the lower wavelength region confirmed the formation of a nanosized product. The optical band gap of the material was calculated by effective mass approximation and it was found to be 3.3, 3.42, 3.45 and 3.5 eV for TiO_2 calcined at various temperatures.

3.4 Raman Studies of TiO_2 Nanoparticles

Raman spectra of TiO_2 nanoparticles at 150 °C and annealed a various temperatures from 300 to 600 °C are shown in Fig. 6. TiO_2 nanoparticles have frequently been investigated with Raman spectroscopy because of the unusual band broadening and shifts of Raman bands with decreasing particle size. On the basis of the Heisenberg uncertainty principle, the relationship between particle size and photon position can be expressed as follows:

$$\Delta X\ \Delta P \geq \frac{\hbar}{2}$$

where ΔX is the particle size, ΔP is the phonon momentum distribution, and $\hbar$ is the reduced Planck's constant. As the particle size decreases, the phonon is increasingly confined within the particle and the phonon momentum distribution increases. This broadening of the phonon momentum leads to a broadening of the scattered phonon momentum according to the law of conservation of momentum. This phonon dispersion causes asymmetric broadening and may lead to a shift of the Raman bands [29]. According to factor group analysis, anatase has five Raman bands ($A_{1g}+B_{1g}+3E_g$). It is seen (Fig. 6) that the five allowed modes are at 638.8 (E_g),

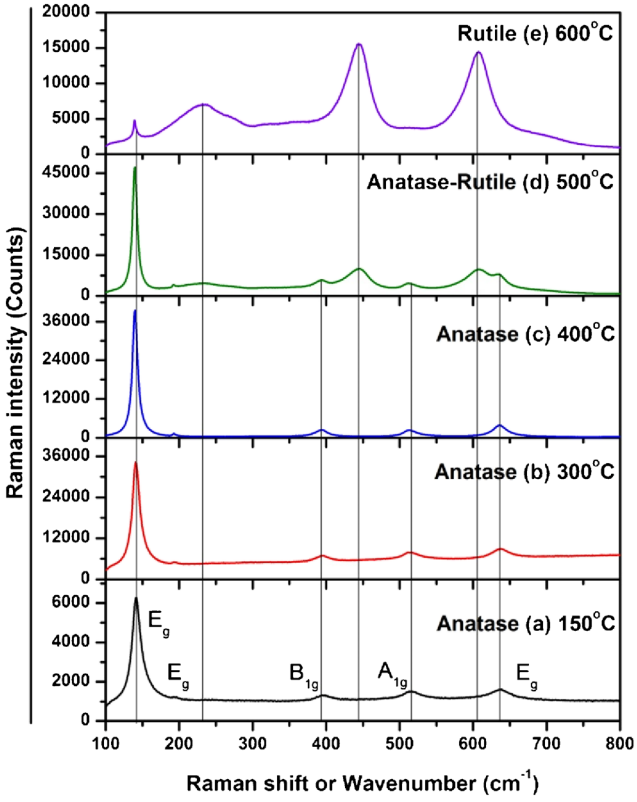

Fig. 6 Raman spectra of TiO_2 nanoparticles

516.0 (A_{1g}) 393.4 (B_{1g}), and 192.4 cm^{-1} (E_g), as well as a very sharp and intense peak at 139.15 (E_g) for temperatures up to 400 °C. The O-O interactions, based on residual valence are calculated to occur in the 252–394 cm^{-1} region.

The broad band observed near 160–240 cm^{-1} is assigned to O-O interactions involving three and four coordinate oxygen. The sharp feature at 139.15 cm^{-1} is consistent with Ti-Ti covalent interactions (2.96 Å; 0.29 valence units). Annealing at 500 °C (Fig. 6d), results in the formation of both anatase and rutile, with anatase the dominant phase in addition to a small amount of rutile. As the annealing temperature is increased from 500 to 600 °C, (Fig. 6d–e), the relative amount of rutile increases as evidenced by the relative intensity increase of the Raman bands and exhibits major peaks at 231.7, 444.3, and 608.2 cm^{-1}. The peaks of crystalline rutile are initially observed for annealing at 600 °C and become shaper and more intense as the annealing temperature is increased, indicating increased crystallinity of the rutile phase.

3.5 Thermal Properties of TiO_2 Nanoparticles

The thermal decomposition, phase transition and phase stability of synthesized TiO_2 nanoparticles were studied by TG-DTA analysis as shown in Fig. 7. In TiO_2 particles

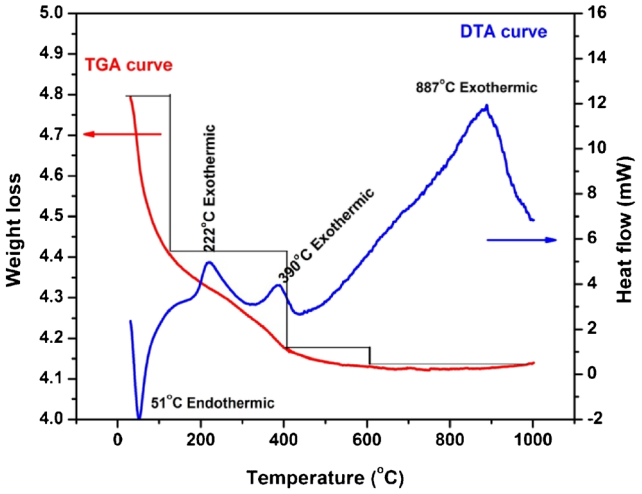

Fig. 7 TGA-DTA curves of TiO_2 nanoparticles

the weight loss occurred in three stages. From the TG-DTA the weight loss was observed in TiO_2 particles at around 0–122, and 122–403, and 403–900 °C. The first weight loss occurred around 0–122 °C which is due to loss of moisture and water molecules. In the FTIR spectra the bands observed at 1600 cm^{-1} and 3400 cm^{-1} clearly show the presence of water molecules. The second weight loss observed between 122–403 °C shows the loss of organic residues and organic polymer compounds. The weight loss is attributed to the combustion of organic compounds, that is the weight reduction is due to the loss of carbon, hydrogen and oxygen. After that there was a third weight loss observed at around 403–610 °C, probably due to the phase transformation of amorphous to crystalline anatase phase. The fourth weight loss was observed around 850–900 °C, which is attributed to the further phase transformation of anatase phase to rutile phase. From the TG-DTA analysis another phase i.e. rutile phase was also observed around 850–900 °C. In XRD analysis, anatase phase was changed to rutile in the samples annealed at above 500 °C. The DTA curve distinctly shows two exothermic peaks and one endothermic peak, the first and second peaks at 222 °C and 390 °C are due to the decomposition of water and residual organic compounds and added surfactants during the synthetic process, while the second sharp peak at 887 °C is due to the crystallization of TiO_2.

4 Conclusions

Titanium oxide (TiO_2) nanoparticles were synthesized by a simple precipitation method. The structural, surface, optical and thermal properties of TiO_2 nanoparticles were investigated. The peaks corresponding to anatase and rutile TiO_2 are evident from XRD and the average particle size and morphologies were studied by TEM. FTIR showed various functional groups in TiO_2 nanoparticles were identified and determined by the transmission and absorption range. The shift in the absorption edge toward lower wavelength indicates the quantum confinement effect with a band gap found to be 3.2 eV. Photoluminescence of the as-prepared TiO_2 nanoparticles was observed and investigated. The sharp UV emission at 421 nm is probably related to the recombination of the electron-hole pair while the weak emission band at 4383 nm can be ascribed to an electron transition mediated by defects levels in the band gap. The broadening and shifts of Raman bands of the TiO_2 nanoparticles were determined using Raman spectroscopy. The origin of Raman band shifts can be attributed to the phase change from anatase to rutile with temperature increase. TG-DTA indicates that the weight loss was observed in TiO_2 particles at around 0–122, and 122–403, and 403–900 °C. Hence, it was confirmed that the synthesized TiO_2 nanoparticles were suitable for photocatalytic and optoelectrics device applications.

Acknowledgements The authors give grateful thanks to the TEM facility for Sophisticated Test and Instrumentation Centre, Cochin, XRD, PL, TGA and Raman Spectroscopy for IISc, Bangalore, and FTIR, UV for Government Engineering College, Burgur, for providing instrument facilities.

References

1. Balachandaran K, Venckatesh R, Sivaraj R (2010) Synthesis of Nano TiO_2-SiO_2 composite using sol-gel method: effect on size, surface morphology and thermal stability. Int J Eng Sci Technol 2:3695–3700
2. Tang Z, Kotov NA, Giersig M (2002) Spontaneous organization of single CdTe nanoparticles into luminescent nanowires. Science 297:237–240
3. Campbell CT, Parker SC, Starr DE (2002) The effect of size-dependent nanoparticle energetics on catalyst sintering. Science 25:811–814
4. Emerich DF, Thanos CG (2003) Nanotechnology and medicine. Expert Opin Biol Ther 3:655–663
5. Pan ZW, Dai ZR, Wang ZL (2001) Nanobelts of semiconducting oxides. Science 9:1947–1949
6. Dong LF, Cui ZL, Zhang ZK (1997) Gas sensing properties of nano-ZnO prepared by arc plasma method. Nanostruct Mater 8:815–823
7. Pal M, Serrano JG, Santiago P, Pal U (2007) Size-controlled synthesis of spherical TiO2 nanoparticles: morphology, crystallization, and phase transition. J Phys Chem C 111:96–102
8. Chena Y-F, Leec C-Y, Yenga M-Y, Chiua H-T (2003) The effect of calcination temperature on the crystallinity of TiO_2 nanopowders. J Cryst Growth 247:363–370
9. Diebold U (2003) The surface science of titanium dioxide. Surf Sci Rep 48:53–229
10. Comini E, Ferroni M, Guidi V, Faglia G, Martinelli G, Sberveglieri G (2002) Nanostructured mixed oxides compounds for gas sensing applications. Sens Actuators B Chem 84:26–32
11. Zeng W, Liu T, Wang Z, Tsukimoto S, Saito M, Ikuhara Y (2010) Oxygen adsorption on anatase TiO_2 (101) and (001) surfaces from first principles. Mater Trans 51:171–175

12. Pradhan SS, Pradhan SK, Bhavanasi V, Sahoo S, Sarangi SN, Anwar S, Barhai PK, Pradhan SS (2012) Low temperature stabilized rutile phase TiO_2 films grown by sputtering. Thin Solid Films 520:1809
13. Ali A, Zareen S, Irfan M (2014) The effect of annealing temperatures on phase and optical properties of TiO_2 nanoparticles for solar cell applications. Eur Sci J 2:447–450
14. Wang W, Gu B, Liang L, Hamilton WA, Wesolowski DJ (2004) Synthesis of Rutile α-TiO_2 nanocrystals with controlled size and shape by low-temperature hydrolysis: effects of solvent composition. J Phys Chem B 108:14789–14792
15. Kanna M, Wongnawa S (2008) Mixed amorphous and nanocrystalline TiO_2 powders prepared by sol–gel method: characterization and photocatalytic study. Mater Chem Phys 110:166–175
16. Hidalgo MC, Bahnemann D (2005) Highly photoactive supported TiO_2 prepared by thermal hydrolysis of $TiOSO_4$: optimisation of the method and comparison with other synthetic routes. Appl Catal B Environ 61:259–266
17. Xia XH, Liang Y, Wang Z, Fan J, Luo YS, Jia ZJ (2008) Synthesis and photocatalytic properties of TiO2 nanostructures. Mater Res Bull 43:2187–2195
18. Zhang X, Zhou M, Lei L (2005) Preparation of anatase TiO_2 supported on alumina by different metal organic chemical vapor deposition methods. Appl Catal A Gen 282:285–293
19. Banerjee I, Karmakar S, Kulkarni NV, Nawale AB, Mathe VL, Das AK, Bhoraskar SV (2010) Effect of ambient pressure on the crystalline phase of nano TiO_2 particles synthesized by a dc thermal plasma reactor. J Nanopart Res 12:581–590
20. Mohammadi MR, Fray DJ, Cordero-Cabrera MC (2007) Sensor performance of nanostructured TiO_2 thin films derived from particulate sol–gel route and polymeric fugitive agents. Sens Actuators B 124:74–83
21. Dennis Christy P, NirmalaJothi NS, Melikechi N, Sagayaraj P (2009) Synthesis, structural and optical properties of well dispersed anatase TiO_2 nanoparticles by non-hydrothermal method. Cryst Res Technol 44:484–488
22. Liao MH, Hsu CH, Chen DH (2006) Preparation and properties of amorphous titania-coated zinc oxide nanoparticles. J Solid State Chem 179:2020–2026
23. Xie Y, Liu X, Huang A., Ding C, Chu PK (2005) Improvement of surface bioactivity on titanium by water and hydrogen plasma immersion ion implantation. Biomaterials 26:6129–6135
24. Dong J, Yao X, Bo H, Dong W, Yuhan S (2008) A simple non-aqueous route to anatase TiO_2. Eur J Inorg Chem 2008:1236–1240
25. Malladi S, Mallikarjunagouda BP, Ravindra SV, Sangamesh AP, Tejraj MA (2006) Novel dense poly (vinyl alcohol)–TiO_2 mixed matrix membranes for pervaporation separation of water–isopropanol mixtures at 30 °C. J Mem Sci 281:95–102
26. Colombo DP Jr, Roussel KA, Sach J, Skinner DE, Cavaleri JJ, Bowman RM (1995) Chem Phys Lett 232:207
27. Dennis Christy P, NirmalaJothi NS, Melikechi N, Sagayaraj P (2009) Synthesis, structural and optical properties of well dispersed anatase TiO_2 nanoparticles by non-hydrothermal method. Cryst Res Technol 44:484–488
28. Khanna PK, Singh N, Shobhit C (2007) Synthesis of nanoparticles of anatase-TiO_2 and preparation of its optically transparent film in PVA. Mat Lett 61:4725–4730
29. Choi HC, Jung YM, Kim SB (2005) Size effects in the Raman spectra of TiO_2 nanoparticles. Vib Spectrosc 37:33–38